

# Polyimides Containing Phosphaphenanthrene Skeleton: Gas-Transport Properties and Molecular Dynamics Simulations

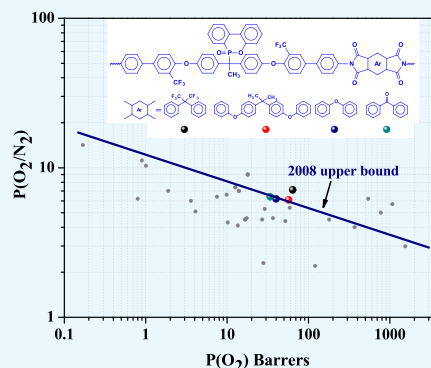
Rimpa Chatterjee,<sup>†</sup> Soumendu Bisoi,<sup>†</sup> Anaparthi Ganesh Kumar,<sup>†</sup> Venkat Padmanabhan,<sup>‡</sup> and Susanta Banerjee<sup>\*,†</sup>

<sup>†</sup>Materials Science Centre, Indian Institute of Technology Kharagpur, Kharagpur 721302, India

<sup>‡</sup>Department of Chemical Engineering, Tennessee Technological University, Cookeville, Tennessee 38505, United States

## S Supporting Information

**ABSTRACT:** A series of new semifluorinated polyimide (PI) films with phosphaphenanthrene skeleton were prepared by thermal imidization of poly(amic acid)s derived from a diamine monomer: 1,1-bis[2'-trifluoromethyl-4'-(4"-aminophenyl)phenoxy]-1-(6-oxido-6H-dibenz(c,e)(1,2)oxaphosphorin-6-yl)ethane on reaction with four structurally different aromatic dianhydrides. The chemical structures of the polymers were established by Fourier transform infrared and <sup>1</sup>H NMR spectroscopy techniques. The polymers showed a good combination of thermal and mechanical properties ( $T_{d10}$  up to 416 °C under synthetic air and tensile strength up to 91 MPa), low dielectric constant (2.10–2.55 at 1 MHz), and  $T_g$  values as high as 261 °C. Gas permeabilities of these films were investigated for four different gases CO<sub>2</sub>, O<sub>2</sub>, N<sub>2</sub>, and CH<sub>4</sub>. The PI films showed high gas permeability ( $P_{CO_2}$  up to 175 and  $P_{O_2}$  up to 64 barrer) with high permselectivity ( $P_{CO_2}/P_{CH_4}$  up to 51 and  $P_{O_2}/P_{N_2}$  up to 7.1), and the values are better than those of many other similar polymers reported earlier. For the O<sub>2</sub>/N<sub>2</sub> gas pair, the PIs (PI A) surpassed the present upper boundary limit drawn by Robeson. A detailed molecular dynamics (MD) simulation study has been conducted to understand better the gas-transport properties. The effect of phosphaphenanthrene skeleton, its spatial arrangement, and size distribution function of the free volume were studied using molecular dynamics (MD) simulation and the results are correlated with the experimental data.



## INTRODUCTION

Membrane-based separation technology plays a key role in many industrial and scientific areas as it offers many advantages over other technologies.<sup>1–5</sup> Therefore, gas separation using polymer membranes has successfully been employed in a variety of applications like O<sub>2</sub> or N<sub>2</sub> enrichment of air (separation of air for O<sub>2</sub> enrichment in combustion processes or medical applications and N<sub>2</sub> enrichment for prevention of oxidation), natural gas “sweetening” (removal of CO<sub>2</sub>), hydrogen recovery from ammonia manufacture (separating H<sub>2</sub> from N<sub>2</sub>), and post-combustion capture of CO<sub>2</sub> (separating CO<sub>2</sub> from N<sub>2</sub>).<sup>6–9</sup> However, large precursor material associated with high production cost, difficulties in obtaining highly pure product, and inadequate thermal and chemical stabilities of many polymer membranes in separation condition are the main reasons that limited the full development of membrane-based separation applications.<sup>4</sup> Additionally, high-efficiency gas separation demands such kind of membrane materials that possess good selectivity for one gas over another, along with high permeability. Higher permeability decreases the amount of membrane area required to treat a given amount of gas, thereby decreasing the capital cost of membrane units. Higher selectivity results in higher-purity product gas.<sup>10</sup> Nevertheless, there exist a trade-off relation between permeability ( $P$ ) and selectivity ( $\alpha$ ), i.e., polymer membranes with high permeability usually display

poor selectivity and vice versa.<sup>11,12</sup> This point was first recognized by Robeson with Freeman, and a theoretical basis for this behavior was developed later.<sup>10,12,13</sup> Generally, polymers used for commercial gas-separation membranes like Matrimid or Ultem possess high selectivity, but low permeability.<sup>14</sup> Thus, the key paradigm of our research interest is designing new polymeric membranes with both high permeability and permselectivity for the different gas pairs (CO<sub>2</sub>/CH<sub>4</sub>, O<sub>2</sub>/N<sub>2</sub>, etc.) with good thermal, mechanical, and chemical stabilities. This attempt led the researchers to thoroughly examine the chemical and physical properties of the polymers, which are essential to separate a particular gas mixture.<sup>15</sup>

Practically, there is no “design rule” for optimal gas permeation and its relationship with polymer chemical structure.<sup>16</sup> But several studies have reported<sup>12,16–18</sup> structural modification through comparatively rigid structure that leads to increase in fractional free volume (FFV) (by disrupting chain packing via introducing bulky groups to increase interchain spacing) and reduces rotational agility around flexible linkages, which helped in improving both permeability and permselectivity. Additionally, for practical application, the polymer

Received: June 18, 2018

Accepted: September 28, 2018

Published: October 18, 2018

Scheme 1. Scheme of Synthesis of PIs (A–D)

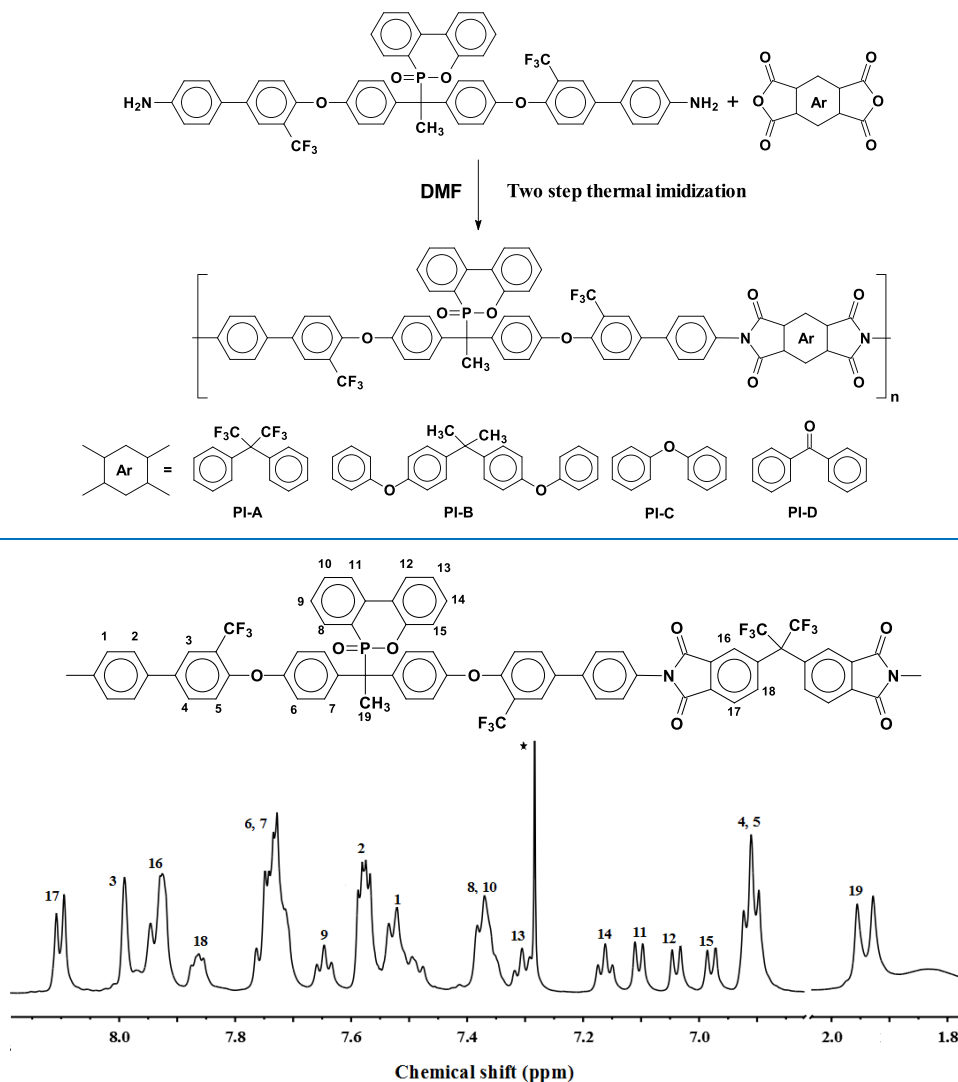


Figure 1. Representative  $^1\text{H}$  NMR spectrum of PI A in  $\text{CDCl}_3$  (\* corresponds to the proton of  $\text{CHCl}_3$ ).

membrane must be thermally, mechanically, and chemically stable.<sup>19</sup>

In this context, aromatic polyimides (PIs) are well known as high-performance membrane materials due to their strong size-sieving ability as well as excellent mechanical, thermal, and chemical stabilities and structural diversity.<sup>20–22</sup> Moreover, polyimides exhibit good selectivity for a number of gas pairs (e.g.,  $\text{CO}_2/\text{CH}_4$ ,  $\text{H}_2/\text{CH}_4$ ,  $\text{H}_2/\text{CO}$ ,  $\text{O}_2/\text{N}_2$ , etc.). Therefore, polyimides are a good choice for membrane-based gas-separation applications.<sup>14</sup> However, their insolubility in common organic solvents and infusible nature prevents membrane preparation by both solution casting and melt processing routes.<sup>19</sup> Numerous studies have been carried out to adjust the interchain interaction of polyimides so that they can be easily processed by either solvent casting or melt processing.<sup>23</sup> These studies lead toward the modification of the polymer backbone by introducing a bulky substituent, fluorine-containing unit, flexible linkage, etc. In this respect, phosphorus-functionalized polymers in the phosphinate form have drawn attention because of their improved thermal properties and low flammability.<sup>24</sup> Recently, polymers containing 9,10-dihydro-9-oxa-10-phosphaphenanthrene 10-oxide

(DOPO) have received much attention. This bulky structure is free of conformational stress and prevents packing of polymer chains. A large number of compounds with phosphaphenanthrene skeleton were produced by reacting the active hydrogen of DOPO with several of electron-deficient compounds.<sup>25</sup> DOPO moieties in polyimide chain improve polymer solubility, thermal stability, and flame retardancy.<sup>26,27</sup> Additionally, introduction of pendant trifluoromethyl ( $-\text{CF}_3$ ) groups hinders close packing of the polymer chains, which leads to increase of free volume as a result gas permeability increase and improvement of the processibility of polyimides.<sup>19</sup> Accounting both high permeability and selectivity, fluorinated polymers are superior contenders in comparison to nonfluorinated ones.<sup>28</sup> Fluorine-containing polymers are also known for low dielectric constant, low water absorption, and high optical transparency. Recently, our group has reported the gas-transport properties of polyamides with phosphaphenanthrene skeleton with high gas permeability.<sup>29</sup>

In the present study, we report the synthesis of a series of new polyimides with phosphaphenanthrene group and their thorough characterization by spectroscopic methods like  $^1\text{H}$  NMR and Fourier transform infrared (FTIR) spectroscopies.

Table 1. Physical Properties of the Polyimides

polymer	$\eta_{inh}$ (dL/g) <sup>a</sup>	$M_n$ <sup>b</sup> (g/mol)	PDI	density (g/cm <sup>3</sup> )	$V_w$ (cm <sup>3</sup> ) <sup>c</sup>	FFV <sup>d</sup>	FFV <sup>SIM</sup>	$\epsilon^e$	water absorption at 30 °C (%)	fluorine content (%)
PI A	1.14	60 400	2.2	1.11	0.472	0.319	0.372	2.10	0.44	17.44
PI B	1.15	62 200	2.4	1.21	0.437	0.310	0.341	2.55	0.59	8.24
PI C	0.97	55 100	2.7	1.17	0.485	0.262	0.287	2.37	0.48	9.72
PI D	n.d.	n.d.	n.d.	1.22	0.476	0.245	0.264	2.41	0.51	9.62

<sup>a</sup>Inherent viscosity at 30 °C. <sup>b</sup>Number-average molecular weight. <sup>c</sup>Specific van der Waals volume estimated using HyperChem computer program, version 7.0. <sup>d</sup>FFV is the fractional free volume determined from Bondi's formula. FFV<sup>SIM</sup> is the FFV values of the PIs determined from atomistic molecular dynamics (MD) simulations. <sup>e</sup>Dielectric constant at 1 MHz frequency and 30 °C.

Thermal, mechanical, and gas-transport properties of the polymers were also investigated. To understand the performance of polymers as gas-separation membranes, the gas permeability values are plotted in Robeson diagrams. Molecular dynamics (MD) simulation at the atomistic level has been performed to understand the structural orientations of polymers and their effect on the gas-transport properties of penetrant gas molecules in polymer matrices. The dynamic properties of the microstructure like trajectories of gas molecules and the diffusion behavior of the penetrant molecules are also investigated.

## RESULTS AND DISCUSSION

**Synthesis and Characterization.** Several new PIs with phosphaphenanthrene skeleton (PI A, PI B, PI C, and PI D) were synthesized by reacting 1,1-bis[2'-trifluoromethyl-4'-(4'-aminophenyl)phenoxy]-1-(6-oxido-6H-dibenz(c,e)(1,2)oxaphosphorin-6-yl)ethane with four structurally different aromatic dianhydrides in *N,N*-dimethylformamide (DMF) by a two-step procedure, e.g., ring-opening polyaddition of cyclic dianhydrides with diamine to form poly(amic acid)s (PAAs), followed by thermal cyclization, as shown in Scheme 1.

Experimentally determined C, H, F, N, O, and P contents of the PIs and values calculated from their repeat unit structures were in good agreement. The <sup>1</sup>H NMR spectra of the PIs confirmed their repeat unit structures in terms of available magnetically different protons and their relative intensities. The <sup>1</sup>H NMR spectrum of PI A in CDCl<sub>3</sub> is shown in Figure 1 as a representative one. The <sup>1</sup>H NMR spectra of the PIs did not show any peak corresponding to free amine or amide protons, indicating the high conversion of the monomers and complete imidization.<sup>30</sup>

The FTIR spectra of the PIs showed characteristic absorption bands at ~1780 cm<sup>-1</sup> (asymmetric >C=O stretching) and ~1690 cm<sup>-1</sup> (symmetric >C=O stretching), indicating the formation of imide linkages. The absence of characteristic stretching bands near 3200 cm<sup>-1</sup> (–OH stretching) and 3350 cm<sup>-1</sup> (>N–H stretching) of the PAAs supported complete imidization. The bands near ~1360 cm<sup>-1</sup> (C–N symmetric stretching) and ~820 cm<sup>-1</sup> (C–N bending) also supported the successful formation of imide linkages and high conversion of the monomers to polymers. Other characteristic bands are ~1620 cm<sup>-1</sup> (aromatic >C=C< stretching), ~1483 cm<sup>-1</sup>, ~1366 cm<sup>-1</sup> (asymmetric C–O–C stretching), ~1230 cm<sup>-1</sup>, ~1130 cm<sup>-1</sup> (C–F stretching), and ~1060 cm<sup>-1</sup> (C–O–C symmetric stretching).

The solubility of the PIs was investigated in different organic solvents at a concentration of 10% (w/v) at room temperature. All of the polymers (except PI D) were soluble in many common organic solvents, such as dimethylacetamide, 1-methyl-2-pyrrolidone (NMP), DMF, and dimethyl sulfoxide, as well as in many low-boiling solvents like tetrahydrofuran (THF),

dichloromethane, and CHCl<sub>3</sub>. The presence of a bulky phosphaphenanthrene skeleton, pendant –CF<sub>3</sub> group, and flexible spacer like ether linkage in the polymer backbone inhibits close packing, leading to polymer chain–chain interaction, which is attributed to their high free volume and improved solubility.<sup>31</sup> The PIs with additional ether linkages (PI B and PI C) or hexafluoroisopropylidene linkage (PI A) in the dianhydride part exhibited improved solubility. However, the 3,3',4,4'-benzophenonetetracarboxylic dianhydride (BTDA)-based polymer (PI D) was insoluble in such organic solvents and in agreement with the previous reports. The insolubility of the BPDA-based polyimides was attributed to the formation of network structure through the reaction of the carbonyl group in 4,4'-(4,4'-isopropylidenediphenoxy)bis(phthalic anhydride) (BPADA) with the amine groups during high-temperature thermal imidization.<sup>32,33</sup>

The physical properties of the polymers are summarized in Table 1. The inherent viscosities ( $\eta_{inh}$ ) of the PIs are in the range of 0.97–1.15 dL/g in NMP, indicating the formation of high molar mass polymers. The number-average molecular weight of the polymers is more than 55 000 g/mol, and the values are in accordance with the viscosity values. The polydispersity index values were also in the ranges as usually obtained in traditional step-growth polymerization.<sup>30</sup> The density values of the polymer films were in the range of 1.11–1.22 g/cm<sup>3</sup>. The bulky phosphaphenanthrene moiety is free of conformational stress and prevents packing of polymer chains and leads to decrease of the density of the polymer films and thereby increase of free volume.<sup>29</sup> Additionally, large hexafluoroisopropylidene groups further inhibit close chain packing (thereby inhibiting the rotational mobility of the polymer chain) and therefore the 4,4'-(hexafluoroisopropylidene)diphthalic anhydride (6FDA)-based polymers (PI A) have the highest FFV within this series of polyimides.<sup>34</sup> However, the obtained experimental FFV values (especially for PI A and PI B) seem to be unusually high, similar to those reported for high free volume, highly permeable polymers like PTMSP and AF2400.<sup>35</sup> Determining the reasons for this requires further corroboration and elucidation.

The interchain packing of the polymer membranes was investigated by out-of-plane wide-angle X-ray diffraction (WAXD) measurements. The broad X-ray diffractogram of the PIs (Figure 2) indicated their amorphous nature. The amorphous nature of the PIs is due to the presence of an unsymmetrical phosphaphenanthrene skeleton, bulky trifluoromethyl groups in the diamine structure. All of these structural units disturbed regularity and hindered close packing of polymer chain. On the WAXD pattern, the position and shape of the amorphous halo were dependent on the type of dianhydrides used during polymerization. Different diffraction patterns in WAXD provide different free volume morphologies, which affects FFV and gas permeability of the polymers.

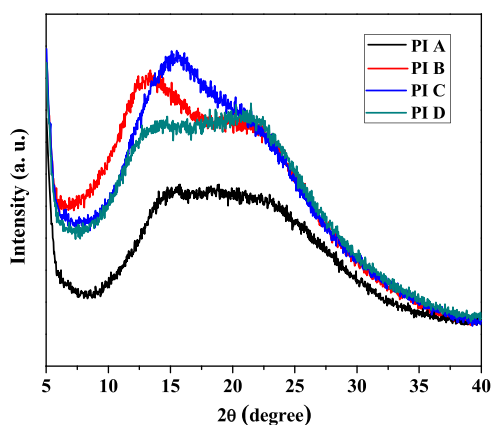


Figure 2. WAXD patterns of the polyimide membranes.

Water absorption behavior is one of the important parameters for the polymers used in electronic packaging applications, as the absorbed water affects their dielectric performance.<sup>36</sup> The water absorption value for PIs ranges from 0.44 to 0.59% (Table 1). The polyimides derived from 6FDA (PI A) showed the lowest water absorption (0.44%). This was attributed to the higher fluorine content in PI A.<sup>19</sup> The water uptake values of these PIs were less than those of Ultem 1000 (1.52%) and Kapton (3%).<sup>37,38</sup>

Polyimides are typically used in interlayer dielectrics as gap fill materials.<sup>19</sup> Therefore, it is always an interest to know the dielectric constant values of newly prepared polyimides. Accordingly, the dielectric constants ( $\epsilon$ ) of these polymer membranes were measured using a dielectric meter at 1 MHz frequency, 30 °C, and relative humidity of 45%. The polymer films showed considerably low dielectric constant values between 2.10 and 2.55 (Table 1). It is attributed that the bulky phosphaphenanthrene moiety and pendent  $-\text{CF}_3$  groups prevent close packing of the polymer chains, which increases the fractional free volume and decreases the number of polarizable units per unit volume. Another important factor is that the electronic polarizability of C–F bond is lower than that of C–H bond (bond polarizability, C–F = 0.56 and C–H = 0.65 units). This also contributes to the reduction of  $\epsilon$  values related to the fluorine content in the polymers. Therefore, PI A having the highest fluorine content showed the lowest  $\epsilon$  value ( $\epsilon = 2.10$ ) in the series. It should also be noted that the dielectric constant values of these polymers were considerably lower than those of many other nonfluorinated polyimides, e.g., Kapton H ( $\epsilon = 3.5$  at 1 kHz), Upilex R ( $\epsilon = 3.5$  at 1 kHz), Upilex S ( $\epsilon = 3.5$  at 1 kHz), and Ultem 1000 ( $\epsilon = 3.15$  at 1 kHz), and comparable to those of many semifluorinated poly(ether imide)s, e.g., 6FDA-*m*-phenylene diamine (MPD,  $\epsilon = 3.0$ ); 6FDA-7FMEDA ( $\epsilon = 2.9$ ); and 6FDA-13FMEDA ( $\epsilon = 2.7$ ).<sup>37–39</sup>

**Thermal Properties.** The thermal degradation of the polymers is a very important parameter for membrane-based application.<sup>40</sup> Thermal performance of the polymers was assessed by thermogravimetric analysis (TGA) under synthetic air. The TGA images of the polymers are displayed in Figure 3. The PIs revealed a two-step thermal decomposition with 10% weight loss ( $T_{d10}$ ) ranging from 390 to 416 °C in synthetic air (Table 2). The first stage of decomposition ranges from 370 to 440 °C; this is due to the decomposition of P–O bond. The second decomposition stage occurring from 490 to 560 °C is accredited to the decomposition of aromatic polymer chain. The P–C bond is weakest in DOPO, and the O=P–O group was

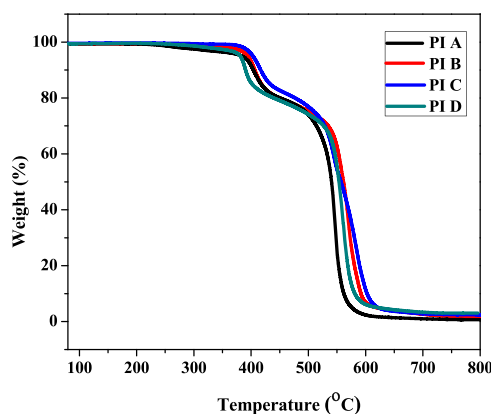


Figure 3. TGA images of the PIs in synthetic air (heating rate: 10 °C/min).

Table 2. Thermal and Mechanical Properties of the Polyimides

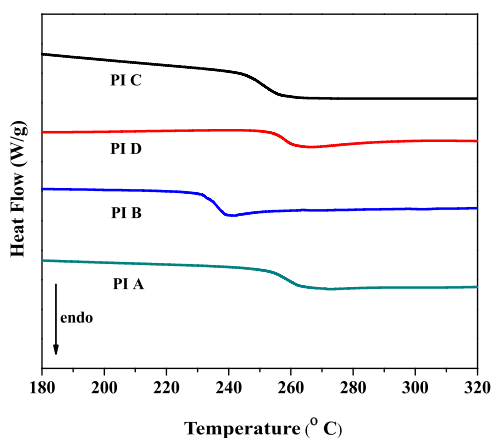
polymer	$T_{d10}$ (°C) <sup>a</sup>	$T_g$ (°C) <sup>b</sup>	T.S. (MPa) <sup>c</sup>	Y.M. (GPa) <sup>d</sup>	E.B. (%) <sup>e</sup>
PI A	416	261	91	1.91	9
PI B	403	235	83	1.59	18
PI C	406	251	70	1.48	13
PI D	390	258	79	1.89	7

<sup>a</sup>10% degradation temperature in air. <sup>b</sup>Glass-transition temperature. <sup>c</sup>Tensile strength. <sup>d</sup>Young's modulus. <sup>e</sup>Elongation at break.

more thermally stable due to the protection of phenylene groups. In DOPO moiety, electron-withdrawing P=O group destabilizes the P–C bond by reducing the electron density of the carbon and an electron-donating methyl group increases the electron density of the carbon. However, the increment of the electron density of aliphatic carbon adjacent to the phosphorous is more compared to the electron-withdrawing P=O group.<sup>29</sup> Therefore, the thermal stability of P–C linkages in DOPO-containing PIs is high. All of these PIs showed residues at 800 °C in the range of 3–4% (considering  $\text{P}_2\text{O}_5$  as the final product).

In this series, PI A showed the highest  $T_{d10}$  compared to other members in this series; this is due to the presence of hexafluoroisopropylidene (6F) moiety in the polymer structure, which has a rigid structure and higher degree of aromaticity that contribute to higher thermal stability. Comparatively lower  $T_{d10}$  values of PI B and PI C are attributed to the presence of oxidizable isopropylidene linkages and the more number of flexible ether linkages in their anhydride moiety.<sup>19</sup>

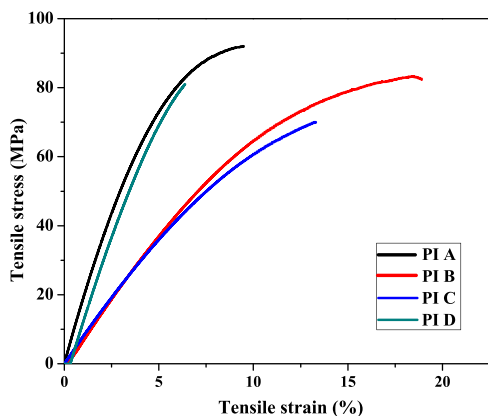
The glass-transition temperatures ( $T_g$ ) of the PIs were determined by differential scanning calorimetry (DSC) under nitrogen atmosphere. The polymers showed glass-transition temperatures without any melting or crystallization transition, indicating their amorphous or glassy morphology. The glass-transition temperature values of the PIs are given in Table 2, and the DSC curves are shown in Figure 4. The  $T_g$  values of the PIs ranged from 235 to 261 °C and followed the order: PI A > PI D > PI C > PI B. Glass-transition temperatures of polymers depend on different factors such as polymer intermolecular force, symmetry, and rigidity of the polymer backbone. It is well known that the glass-transition temperature increases with increasing rigidity. PI A, i.e., 6FDA-based polymers, showed the highest  $T_g$  (261 °C) in this series, which is attributed to the presence of bulky hexafluoroisopropylidene (6F) linkage that hampers the backbone agility and increases rigidity.<sup>38</sup> The presence of additional flexible ether linkage in their anhydride part leads to



**Figure 4.** DSC curves (second heat scan) of the PIs (heating rate: 20 °C/min).

lowering of  $T_g$  of PI B and PI C compared to BTDA-based polymer (PI D). The  $T_g$  values of these polymers are higher than those in many commercial poly(ether imide)s, e.g., Ultem 1000 ( $T_g = 217$  °C), based on BPADA and *m*-phenylene diamine (MPD).<sup>37</sup> The bulky pendant groups in the main chain hinder the rotation of chains, and as a result, the  $T_g$  value increases.

**Mechanical Property.** Mechanical stability of the polymers is an important parameter for their membrane-based gas-separation applications.<sup>2,41</sup> For gas-separation applications, it is important to design the polymer as a tough and flexible membrane with certain qualities like high mechanical strength and good thermal stability. The mechanical properties of all of the PIs films are shown in Table 2, an average value of three repeated measurements is taken, and their corresponding stress–strain curve is shown in Figure 5. The PIs showed high



**Figure 5.** Stress–strain plot of the PIs.

tensile strength up to 91 MPa, elongation at break up to 18%, and Young's modulus up to 1.91 GPa. PIs derived from BPADA (PI B) and 4,4'-oxydiphthalic anhydride (ODPA) (PI C) showed higher elongation of break (18 and 13%, respectively) in comparison to another member of the series, which is attributed to the higher number of flexible ether linkage in their structure. Low elongation at break of PI A and PI D was due to highly rigid 6FDA and BTDA moieties.

**Gas-Transport Properties.** The main objective of our current research is to obtain PI membranes with simultaneously high permeability for gases and more selectivity for one gas over another. The mean gas permeability of four different gases

(CO<sub>2</sub>, O<sub>2</sub>, N<sub>2</sub>, and CH<sub>4</sub>) and their ideal selectivity values for different gas pairs are measured at 3.5 bar and 35 °C. The values are summarized in Table 3. The diffusion coefficients and solubility coefficient values along with their solubility selectivity and diffusivity selectivity values are also tabulated in Table 4.

All of the PIs showed high gas permeability and high permselectivity depending on their structure. The gas permeabilities of polymers are influenced by available FFV, flexibility of the polymer chains, kinetic diameter of the permeate molecules, and polymer–penetrant interactions.<sup>42,43</sup> The presence of bulky phosphaphenanthrene moiety in the main chain restricts rotational mobility and hinders close chain packing, which leads to higher FFV. Again, –CF<sub>3</sub> groups in the polymer chain make the polymer more bulky and effectively decreases interchain packing. As a result, FFV increases, which leads to the increase of permeability values. However, high permselectivity is attributed to the rigidity of the chain coming from phosphaphenanthrene skeleton and –CF<sub>3</sub> groups.<sup>44,45</sup>

The order of permeability coefficient of all of the gases through these PI membranes follows the trend  $P(\text{CO}_2) > P(\text{O}_2) > P(\text{N}_2) > P(\text{CH}_4)$ , and it is exactly opposite to the kinetic diameter of the gas molecules, CO<sub>2</sub> (3.3 Å) < O<sub>2</sub> (3.46 Å) < N<sub>2</sub> (3.64 Å) < CH<sub>4</sub> (3.8 Å).<sup>46</sup> The order of gas permeability coefficient with PIs followed the order: PI A > PI B > PI C > PI D, which is in concurrence with their FFV (Table 1). PI A has the highest gas permeability in this series. This is due to the presence of >C(CF<sub>3</sub>)<sub>2</sub> moiety in the dianhydride part, which makes the polymer chain more rigid and hinders close chain packing, as a result of which openness and FFV increase. PI B showed higher permeability than PI C and PI D. The higher gas permeability of BPADA-based polymer (PI B) is due to the presence of higher number of flexible ether linkages<sup>47</sup> and the presence of bulky >C(CH<sub>3</sub>)<sub>2</sub> groups. PI C exhibited higher gas permeability than PI D, which is due to the additional carbonyl linkage present in PI D, which leads to comparatively close packing of polymers. Therefore, the gas permeability through the polymer chain is greatly influenced by the type of dianhydrides used in making the polymers.

It is well established that for a pair of gas, selectivity decreases with increasing permeability.<sup>48–54</sup> But, the permselectivity for CO<sub>2</sub>/CH<sub>4</sub> and O<sub>2</sub>/N<sub>2</sub> gas pairs followed the order: PI A > PI B > PI D > PI C. 6FDA-based polymer (PI A) exhibited very high permeability along with higher selectivity. Higher permselectivity of PI A is due to the presence of >C(CF<sub>3</sub>)<sub>2</sub> groups, which restricted local segmental mobility and hindered torsional motion of the phenyl rings around >C(CF<sub>3</sub>)<sub>2</sub> linkage.<sup>28</sup> It is well known that increase of  $T_g$  leads to increase of rigidity or stiffness of the polymer chain and is expected to result in higher selectivity.

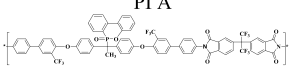
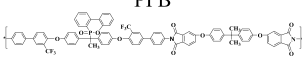
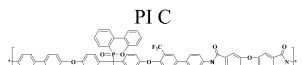
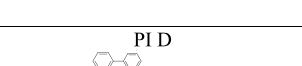
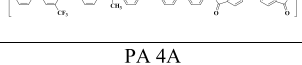
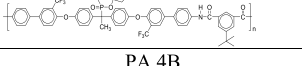
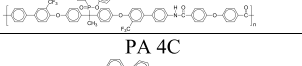
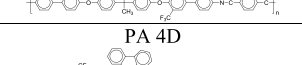
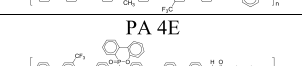
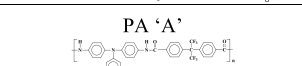

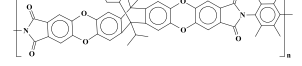
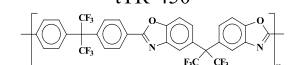
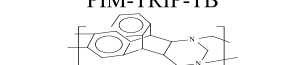
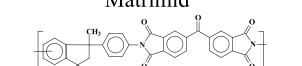
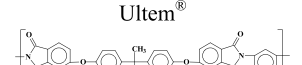
The permeability coefficient values of the polyimides for different gases have been correlated with their FFV. The relation between gas permeability and FFV can be described by eq 1

$$P = A e^{(-B/\text{FFV})} \quad (1)$$

where  $A$  is a preexponential factor and  $B$  is typical of the size of each gas. The logarithm of gas permeability values is plotted against the reciprocal of FFV in Figure 6. The gas permeability of the polymers increases with their FFV values, and almost a linear relationship was noted except for CO<sub>2</sub>.<sup>42</sup>

The gas permeability ( $P$ ) of polymeric membranes is controlled by gas diffusivity and solubility ( $P = D \times S$ ), and the gas diffusivity and solubility are governed by polymer–penetrant dynamics and polymer–penetrant interactions,

Table 3. Gas Permeability Coefficients ( $P$ ) in Barrer and Permselectivities ( $\alpha$ ) of the Polyimides at 35 °C and 3.5 bar

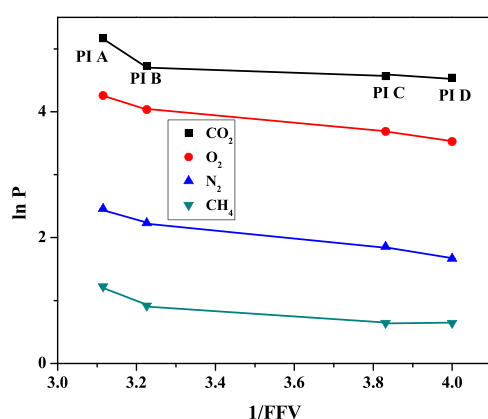
Polymer	$P$ (CO <sub>2</sub> )	$P$ (O <sub>2</sub> )	$P$ (N <sub>2</sub> )	$P$ (CH <sub>4</sub> )	$\alpha$ (CO <sub>2</sub> / CH <sub>4</sub> )	$\alpha$ (O <sub>2</sub> / N <sub>2</sub> )	Ref.
PI A 	175	64	9.0	3.4	51	7.1	a
PI B 	113	57	9.3	2.5	45	6.1	a
PI C 	97	40	6.4	1.9	49	6.2	a
PI D 	94	34	5.3	1.9	48	6.4	a
PA 4A 	164	59.7	11.0	4.1	39.6	5.4	29 <sup>c</sup>
PA 4B 	103	45.5	8.4	2.7	37.7	5.3	29 <sup>c</sup>
PA 4C 	87	34.8	6.7	2.6	33.1	5.2	29 <sup>c</sup>
PA 4D 	81	29.7	5.5	2.0	39.8	5.3	29 <sup>c</sup>
PA 4E 	82	27.8	4.8	1.7	48.7	5.8	29 <sup>c</sup>
PA 'A' 	141	33.4	3.94	3.18	44.33	8.47	48 <sup>c</sup>
KAUST-PI-1 	-	542	-	-	-	6.2	49
tTR-450 	3575	778	155	80.8	44.2	5	50
PIM-TRIP-TB 	-	1073	-	-	-	5.7	49
Matrimid <sup>®</sup> 	8.7	1.9	0.2	0.24	36.0	7.0	51
Ultem <sup>®</sup> 	1.3	0.4	0.05	0.03	36.9	8.0	52
Extem <sup>®</sup> 	3.2	0.8	0.13	0.13	25.2	6.2	53
6FDA-1,4-trip.CF <sub>3</sub>	19.7	5.75	0.99	0.53	37	5.8	54 <sup>d</sup>
6FDA-1,4-trip.para	14.4	4.07	0.66	0.37	39	6.0	54 <sup>d</sup>

$P$  is the gas permeability coefficient in barrer. 1 barrer =  $10^{-10}$  cm<sup>3</sup> (STP) cm/cm<sup>2</sup> s cmHg. <sup>a</sup>This study. <sup>b</sup>Measured at 35° and 3.5 bar. <sup>c</sup>Measured at 35° and 130 psig.

**Table 4.** Gas Diffusion Coefficients,  $D$  ( $10^8$  cm<sup>2</sup>/s), Solubility Coefficients ( $S$ ) in  $10^{-2}$  cm<sup>3</sup> (STP)/cm<sup>3</sup> cmHg, Diffusivity Selectivity ( $\alpha_D$ ), and Solubility Selectivity ( $\alpha_S$ ) Values of the Polyimides<sup>a,b</sup>

polymer	CO <sub>2</sub>		O <sub>2</sub>		N <sub>2</sub>		CH <sub>4</sub>		CO <sub>2</sub> /CH <sub>4</sub>		O <sub>2</sub> /N <sub>2</sub>	
	$D$	$S$	$D$	$S$	$D$	$S$	$D$	$S$	$\alpha_D$	$\alpha_S$	$\alpha_D$	$\alpha_S$
PI A	20.2	8.7	21.7	2.8	6.5	1.5	3.10	1.10	6.51	7.90	3.33	1.86
PI B	17.4	6.5	21.0	2.7	5.9	1.5	2.54	0.98	6.85	6.63	3.55	1.80
PI C	15.5	6.3	16.1	2.5	4.8	1.4	2.20	0.90	7.04	7.00	3.35	1.78
PI D	15.2	6.2	15.6	2.2	5.0	1.2	2.17	0.89	7.00	6.96	3.12	1.83

<sup>a</sup> $D$  is the gas diffusion coefficients in  $10^{-8}$  cm<sup>2</sup>/s. <sup>b</sup> $S$  is the gas solubility coefficients in  $10^{-2}$  cm<sup>3</sup> (STP)/cm<sup>3</sup> cmHg ( $S = P/D$ ).

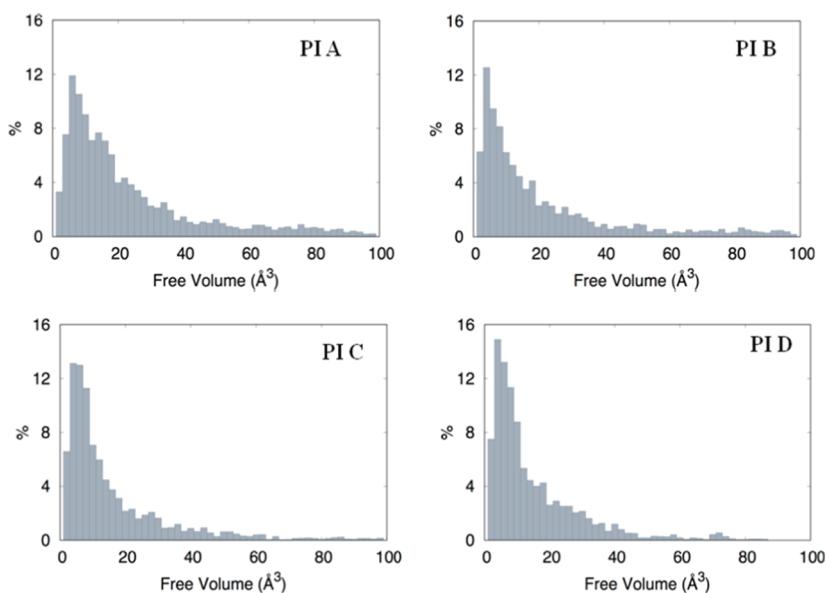


**Figure 6.** Dependence of gas permeability on the reciprocal of fractional free volume of PIs for CO<sub>2</sub>, O<sub>2</sub>, N<sub>2</sub>, and CH<sub>4</sub> gases.

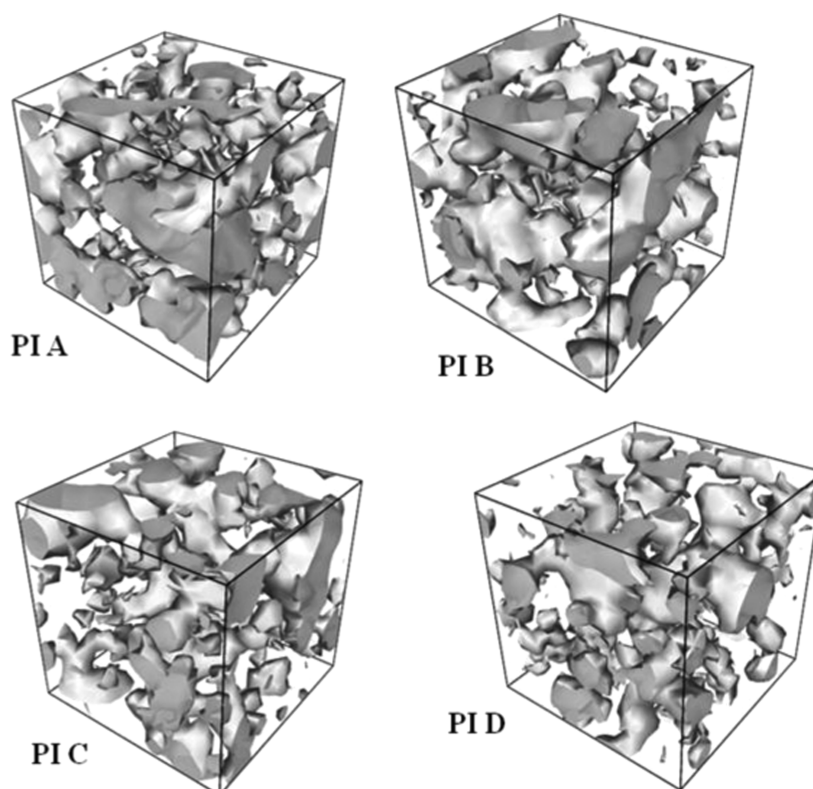
respectively.<sup>29</sup> Therefore, for a better understanding, both the gas diffusivity and solubility coefficients of the PI membranes are determined and the values are presented in Table 4. The gas permeability of the polymers is mainly contributed by their diffusivity coefficient values, rather than the solubility coefficient values of these polymers, particularly for the noncondensable gases. The PIs showed the trend of gas diffusivity as:  $D(\text{O}_2) > D(\text{CO}_2) > D(\text{N}_2) > D(\text{CH}_4)$ , which is not the same as their permeability coefficient values. From the kinetic diameter data, it is expected that CO<sub>2</sub> will diffuse faster compared to O<sub>2</sub>. However, a reverse trend is found and is consistent with many of

the earlier observations.<sup>55</sup> This observation can be explained as follows: there is negligible or no interaction of O<sub>2</sub>, N<sub>2</sub>, and CH<sub>4</sub> with these PIs, but CO<sub>2</sub> has some interaction with the carbonyl or imide groups in the polyimide repeat unit.<sup>56,57</sup> The order of diffusivity coefficients of the PIs followed the same trend as gas permeability coefficients for different PIs, i.e., PI A > PI B > PI C > PI D. The decreasing order of diffusivity coefficient and permeability coefficient corresponds to the decreasing order of FFV values for these PIs. Taking into account the solubility coefficient of the PIs, CO<sub>2</sub> has a higher solubility coefficient than other gases. In comparison to other gases, CO<sub>2</sub> has high permeability due to its high solubility coefficient values.<sup>58</sup> The overall permselectivity is a product of diffusivity selectivity ( $\alpha_D$ ) and solubility selectivity ( $\alpha_S$ ). Permselectivity values of the polyimides for the gas pair CO<sub>2</sub>/CH<sub>4</sub> were predominant by the solubility selectivity as the diffusion selectivity values were relatively low (Table 4). For noninteracting gas molecules like O<sub>2</sub>, N<sub>2</sub>, and CH<sub>4</sub>, permselectivity values are derived from the equal contributions of solubility and diffusivity. For highly soluble and condensable gases such as CO<sub>2</sub>, selectivity is due to solubility selectivity. The solubility coefficients of the PI membranes that arise due to the polymer–penetrant interactions followed the order:  $S(\text{CO}_2) > S(\text{O}_2) > S(\text{N}_2) > S(\text{CH}_4)$ .

**Molecular Dynamics Simulations.** In recent years, with rapidly growing computational resources, simulation has proven to be a very useful tool for better theoretical understanding of the relationship between the chemical structure and transport



**Figure 7.** Size distribution of free volume of the PIs.



**Figure 8.** Free volume morphologies of the polymer membrane matrix estimated for a probe radius of 0.5 Å.

behavior of amorphous polymer membranes as it plays a vital role in membrane science and technology.<sup>59</sup> Molecular dynamics simulation was performed on PI membranes to provide deeper insight into structural orientation of polymer chains and their effect on gas-transport properties.<sup>60</sup> The FFV of the PIs was determined by both atomistic molecular dynamics (MD) simulations (FFV<sup>SIM</sup>) and experiments (FFV). The FFV<sup>SIM</sup> is in the range of 0.264–0.372. It can be observed (Table 1) that the FFV<sup>SIM</sup> value is comparatively higher than FFV, but they follow the same trend PI A > PI B > PI C > PI D. A similar type of observation was also observed by Maya et al.<sup>61</sup> MD simulations provide a better idea of the three-dimensional arrangement, connectivity, and size distribution of free volume elements (FVD) that are not reachable in experiments. Therefore, MD simulations indicated the true free volume of the system. The gas permeability, diffusivity, and permselectivity of polymer membranes are greatly influenced by FVD and the size of free volume elements.<sup>55,62</sup>

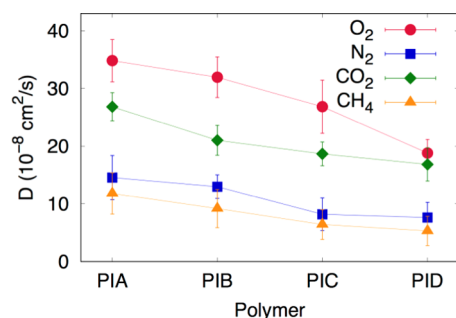
The size distributions of the free volume elements in all of the polymers are given in Figure 7. The FVDs for the PIs helped us to understand the effect of FFV on gas diffusivities in this series of polymers. It is already established that the free volume distributions in amorphous polymers are an important aspect of their transport behavior toward small and medium-sized penetrant molecules.<sup>62</sup> The figure shows the monomodal size distribution with maximum opportunity at free volume element radii of approximately 0–20 Å<sup>3</sup>, which indicates the total extension of an interconnected free volume region.<sup>59</sup> The higher size of free volume distribution is due to the presence of a bulky phosphaphenanthrene moiety, rigid –CF<sub>3</sub> groups, and orientations of polymer chains. Apparently, the spreading appears almost comparable for all of the PI membranes, but in the large-volume radii region, there is a significant difference,

that is, the number of voids with volume larger than 40 Å<sup>3</sup>, highest for PI A and lowest for PI D. PI C and PI D have almost the same distribution after 60 Å<sup>3</sup>. The number of voids with a volume larger than the kinetic diameter of gas molecules has a substantial influence on diffusivity. These plots give an idea of the diffusivity of various gases through these membranes and the accessibility of free volume pockets within the membrane depending on the local arrangement of the polymer chains.

The free volume morphologies of the PI membranes (Figure 8) were analyzed using the free volume size, shape, and connectivity.<sup>59</sup> The gray area in the figure indicates the void spaces in the membrane matrix. In comparison to its amide analogue,<sup>29</sup> the void space is much elongated and connected here. From this observation, it can be concluded that not only bulky phosphaphenanthrene group is accountable for large elongated microcavities in the matrix, but also the structure of the dianhydride part played a vital role. The number and connectivity of void space decrease from PI A to PI D. PI C and PI D have lower void space in comparison to other two polymers, indicating a tight packing of their polymer chain. We can quantitatively correlate free volume morphology with gas permeability of polymer membranes. PI A has the highest void space and well-connected network, and also experimentally, PI A exhibited the highest gas permeability.

The diffusivity order of the four gases through the PI membranes was also determined by molecular dynamic simulations (Figure 9), and it is observed that the experimental value and simulation result follow the same trends to close proximity. This close proximity between the experimental and simulated values signifies the success of our MD simulation for predicting the polymer properties.<sup>6</sup> The trend of diffusion coefficients calculated by MD simulations and experiments was same [ $D(\text{O}_2) > D(\text{CO}_2) > D(\text{N}_2) > D(\text{CH}_4)$ ]. Similar to the

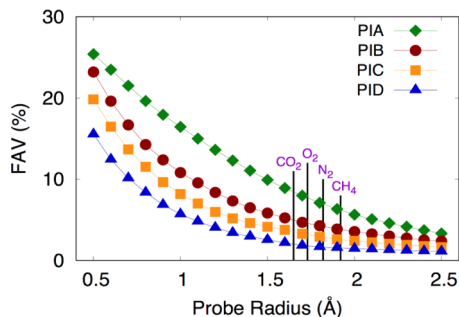




**Figure 9.** Diffusivity order of the four gases through the PI membranes determined by molecular dynamic simulation.

experimental results,  $O_2$  diffuses faster than  $CO_2$ , although  $CO_2$  has smaller size than  $O_2$ . This is attributed to the linear shape of  $CO_2$  molecule, which strongly interacts with the PI membranes and takes comparatively much more time to enter the void space.<sup>63</sup> From Figure 9, it can be seen that PI A has a higher diffusion coefficient in comparison to other PIs in this series. In comparison to the other polymers in the series, the PI A has looser structure and larger FFV, so it provides a pathway with less resistance to diffuse the gas. Therefore, the gas diffusivity is influenced by the size, distribution, and connectivity of the free volume cavities in the membranes and also depends on the shape and interactions of the gas molecules within the matrix.<sup>64</sup>

The fractional accessible volume (FAV) was analyzed using spherical probes with different radii to understand changes in the available free volume with respect to the size of the penetrant molecules. Figure 10 shows the available volume as a function of



**Figure 10.** Fractional accessible volume (FAV) of the different gas molecules for these series of PIs.

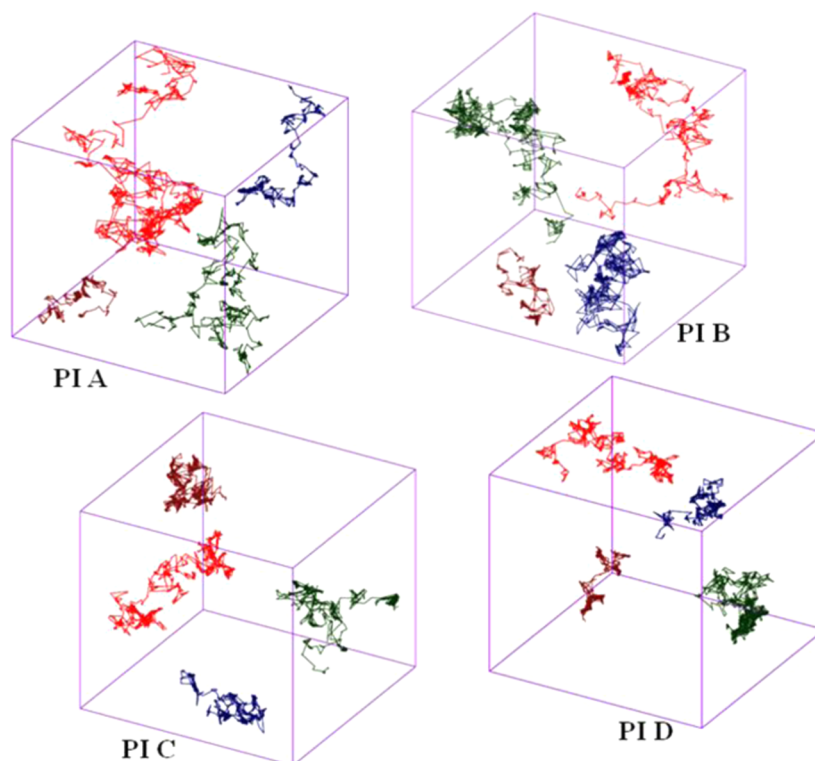
the probe radius. From this figure, it can be observed that the fractional accessible volume is significantly higher in the case of PI A compared to other polymers in the series, which is in good agreement with their FVD (Figure 7). From this figure, it is evident that FAV decreases as probe radius increases and that FFV approaches 0 when the probe radius is larger than approximately 2 Å. The fractional free volume at a probe radius of 0 for all of the polymers ranges from 0.27 to 0.37. This gives the idea that diffusivity of different gases through the polymer membrane is notably different and depends on the effective size of each penetrant molecule. Thus, for larger penetrant molecules like  $N_2$  or  $CH_4$ , gas diffusivity is low in comparison to smaller penetrant molecules such as  $O_2$  and  $CO_2$ . The FAV order follows the same order as FFV PI A > PI B > PI C > PI D. So, the large accessible volume in the polymer matrix increases gas diffusivity as well as improves gas permeability.

To understand the diffusion behavior of the gases through the polymer membrane, the trajectories of gas molecules were further analyzed. The representative trajectories of all of the gas molecules in the simulation box are shown in Figure 11. According to Neyertz et al. the mechanism of transport of gas molecules in the polymer matrix is based on a combination of random oscillations within the available polymer free volumes and occasional jumping events from one void space to another.<sup>65</sup> The largest free volume cavities and a good connectivity between them lead to the highest length of the trajectory for a particular gas molecule in the PI A membrane. The total distance traversed by the gas molecules in the polymer microstructure followed the order ( $O_2$ ) > ( $CO_2$ ) > ( $N_2$ ) > ( $CH_4$ ). The order is in good agreement with the gas diffusivity value. From Figure 11, it is evident that  $O_2$  moves a larger distance in comparison to others (shown by the red line).

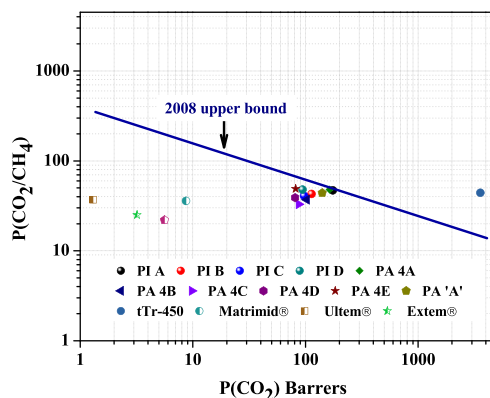
**Comparison of Gas Permeabilities with Previously Reported Polymers.** The ideal gas-separation performances of these polymeric membranes have been compared to those of some commercially available polymer membranes (e.g., Matrimid, Ultem, and Extrem)<sup>51–53</sup> and previously reported polymers.<sup>29,48–50</sup> To better realize the gas-separation performance of the PI membranes, their gas permeability and permselectivity values for a pair of gases were plotted in Robeson diagrams along with many other polymers. It can be seen from Figures 12 and 13 that these polymers showed reasonably high permeability with better separation performances for both  $O_2/N_2$  and  $CO_2/CH_4$  gas pairs compared to Matrimid, Ultem, and Extrem. Especially, PI A showed higher permeability as well as higher permselectivity. For  $O_2/N_2$  gas pairs, all of the synthesized polymers are very close (PI A surpassed) to the upper boundary limit drawn by Robeson.<sup>12</sup>

## CONCLUSIONS

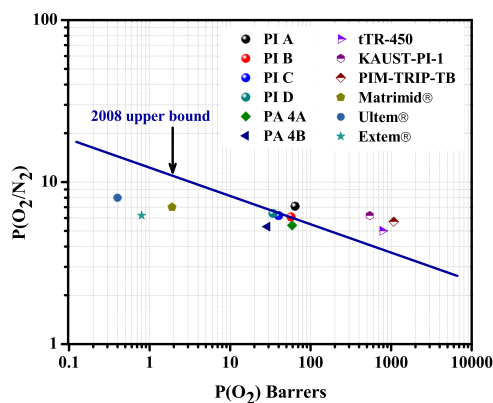
Polyimides are an important class of high-performance polymers because of their excellent thermal and mechanical stabilities and film-forming ability. The introduction of flexible segments like ether linkage and trifluoromethyl ( $-CF_3$ ) or hexafluoroisopropylidene [ $>C(CF_3)_2$ ] groups hinders close packing of the polyimide chains, increases the fractional free volume, and thereby improves the polymer processability and gas permeability.<sup>19</sup> In the present work, a series of polyimide with phosphaphenanthrene unit in the main chain were prepared and characterized in detail. The best combination of thermal and mechanical properties and good film-forming ability made these polymers suitable candidates for membrane-based gas-separation applications. The motivation behind the incorporation of a bulky phosphaphenanthrene unit in the main chain was further to reduce the polymer chain packing, which increases the FFV and simultaneously increases the chain rigidity, thereby manipulating the gas permeability and permselectivity. The polymers showed different fractional free volumes and chain packing depending on the dianhydride structures, and such carefully designed polymers showed improvement in both gas permeability and permselectivity compared to Matrimid or Ultem (which have high selectivity but low permeability). One of the polymers designated as PI A (6FDA-based polymer) showed very good separation efficiency in the series with  $P_{CO_2}$  and  $P_{O_2}$  of 175 and 64 barrer, respectively, and reasonably high permselectivity ( $P_{CO_2}/P_{CH_4} = 51$  and  $P_{O_2}/P_{N_2} = 7.1$ ). All of the polymers showed very high selectivity for  $O_2/N_2$  and placed themselves very close to Robeson upper bound drawn in 2008,



**Figure 11.** Trajectories of gas molecules in PA matrices for a duration of 10 ns at  $T = 30\text{ }^{\circ}\text{C}$ . ( $\text{O}_2 = \text{red}$ ,  $\text{CO}_2 = \text{green}$ ,  $\text{N}_2 = \text{brown}$ ,  $\text{CH}_4 = \text{blue}$ .)



**Figure 12.** Permeability/selectivity trade-off map for  $\text{CO}_2/\text{CH}_4$  separation. Values are from this series of PIs and some other reported polymers.



**Figure 13.** Permeability/selectivity trade-off map for  $\text{O}_2/\text{N}_2$  separation. Values are from this series of PIs and some other reported polymers.

and PI A surpassed the upper boundary limit. Gas diffusivity through these PI membranes was in accordance with the FVD obtained from the computational simulation. The MD study indicated that the overall free volume, free volume distribution, and morphological nature of the polymers play a role in gas permeation. Finally, it can be concluded that using phosphaphenanthrene unit is a good approach to develop PI membranes with a combination of good permeability and selectivity, which is suitable for gas permeation applications.

## EXPERIMENTAL SECTION

**Materials.** 9,10-Dihydro-9-oxa-10-phosphaphenanthrene 10-oxide (DOPO) (>97.0%) was purchased from TCI Chemicals (India). Palladium on activated carbon (1 wt %), tetrakis(triphenylphosphine)palladium(0) (99%), and hydrazine hydrate were purchased from Sigma-Aldrich. Ethanol was purchased from E. Merck, India. All of these chemicals were used without any further purification. 1-Methyl-2-pyrrolidone (NMP) and *N,N*-dimethylformamide (DMF) were purchased from E. Merck, India, stored in NaOH, and distilled from  $\text{P}_2\text{O}_5$  under reduced pressure. Anhydrous  $\text{K}_2\text{CO}_3$  and  $\text{CaCl}_2$  (E. Merck, India) were dried overnight at  $120\text{ }^{\circ}\text{C}$  prior to use. Tetrahydrofuran (THF) was purchased from E. Merck, India, and dried by sodium metal and finally by refluxing over NaH. Toluene (E. Merck, India) was dried by refluxing over sodium metal. The dianhydrides, 4,4'-(hexafluoroisopropylidene)diphthalic anhydride (6FDA), 4,4'-(4,4'-isopropylidenediphenoxy)bis(phthalic anhydride) (BPADA), 4,4'-oxydiphthalic anhydride (ODPA), and 3,3',4,4'-benzophenonetetracarboxylic dianhydride (BTDA) were purchased from Sigma-Aldrich, recrystallized from acetic anhydride, and kept in  $150\text{ }^{\circ}\text{C}$  for 12 h before use. 2,2,4-Trimethylpentane (purity  $\sim 98\%$ , density  $\sim 0.692\text{ g/cc}$ ) was purchased from Sigma-Aldrich.

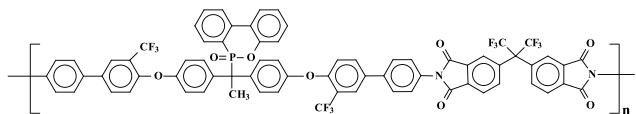
The monomer 1,1-bis[2'-trifluoromethyl-4'-(4"-aminophenyl)phenoxy]-1-(6-oxido-6H-dibenz(*c,e*)(1,2)oxaphosphorin-6-yl)ethane was synthesized according to procedure reported in the literature.<sup>29</sup>

**Synthesis of the Polymers and Membrane Preparation.** The PIs were prepared by reacting the diamine monomer 1-bis[2'-trifluoromethyl-4'-(4"-aminophenyl)phenoxy]-1-(6-oxido-6H-dibenz(*c,e*)(1,2)oxaphosphorin-6-yl)ethane with four different aromatic dianhydrides in *N,N*-dimethylformamide (DMF) (10%, w/v) (Scheme 1). Equimolar amounts of diamine and dianhydride monomers were reacted to get the corresponding poly(amic acid)s (PAA)s, and the corresponding PI membranes were obtained by thermal imidization. The polymerization and preparation of PI A membrane is given below as one of the representatives.

A 25 mL round-bottom flask equipped with a CaCl<sub>2</sub> guard tube and a magnetic stirrer was charged with diamine monomer (0.382 g, 0.425 mmol), 6FDA (0.189 g, 0.425 mmol), and 5 mL dry DMF. The resulting mixture was converted to a viscous PAA solution in 15–20 min and kept under stirring for 1 h. PI membranes were prepared by thermal imidization of the PAA. The viscous PAA solution was cast on a clean, dry, and flat-bottom Petri dish and left overnight at 80 °C for slow evaporation of the maximum amount of solvent. The final cyclization from PAA to PI was achieved by successive heating in 100, 120, 150, 180, 200, and 220 °C for 1 h at each temperature and at 250 °C for 30 min under vacuum. Then, the oven temperature was set at 150 °C and the membranes were kept overnight under vacuum for complete removal of the solvent. Finally, the oven temperature was slowly brought down to room temperature and the membranes were removed from the Petri dishes by putting them in boiling water.

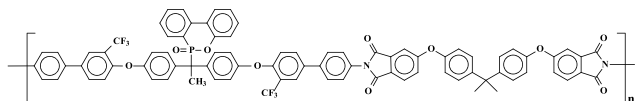
The PI membranes were transparent and flexible with an average thickness of 70 μm. All of the PI membranes were prepared following the same procedure. Analytical details of the PIs are given below.

#### PI A.



Anal. calcd for C<sub>71</sub>H<sub>39</sub>F<sub>12</sub>N<sub>2</sub>O<sub>8</sub>P (1307.03 g/mol): C, 65.24%; H, 3.01%; F, 17.44%; N, 2.14%; O, 9.79%; P, 2.37%. %; found: C, 65.21%; H, 2.99%; F, 17.46%; N, 2.17%; O, 9.76%, P, 2.34%. <sup>1</sup>H NMR (CDCl<sub>3</sub>, 600 MHz, δ ppm): 8.1 (d, *J* = 7.8 Hz, 2H), 7.99 (s, 2H), 7.93 (m, 2H), 7.87 (m, 2H), 7.74 (m, 8H), 7.65 (t, *J* = 7.8 Hz, 1H), 7.56 (m, 4H), 7.52 (m, 4H), 7.37 (m, 2H), 7.3 (t, *J* = 8.0 Hz, 1H), 7.16 (t, *J* = 8.0 Hz, 1H), 7.10 (d, *J* = 8.0 Hz, 1H), 7.04 (d, *J* = 8.0 Hz, 1H), 6.98 (d, *J* = 8.0 Hz, 1H), 6.91 (m, 4H), 1.9 (d, *J* = 16.5 Hz, 3H).

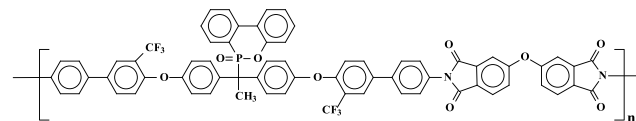
#### PI B.



Anal. calcd for C<sub>83</sub>H<sub>53</sub>F<sub>6</sub>N<sub>2</sub>O<sub>10</sub>P (1383.28 g/mol): C, 72.07%; H, 3.86%; F, 8.24%; N, 2.03%; O, 11.57%; P, 2.24%. %; found: C, 72.04%; H, 3.82%; F, 8.26%; N, 2.01%; O, 11.54%, P, 2.21%. <sup>1</sup>H NMR (CDCl<sub>3</sub>, 600 MHz, δ ppm): 8.06 (d, *J* = 8.2 Hz, 2H), 7.92 (m, 4H), 7.86 (m, 2H), 7.73 (m, 8H), 7.65 (t, *J* = 8 Hz, 1H), 7.59 (m, 6H), 7.52 (m, 6H), 7.37 (d, *J* = 8.4 Hz, 4H), 7.31 (t, *J* = 8.0 Hz, 1H), 7.16 (t, *J* = 8.0 Hz, 1H), 7.10 (d, *J* = 8 Hz,

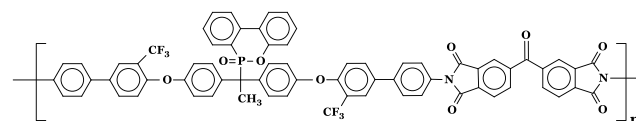
1H), 7.04 (d, *J* = 8.0 Hz, 1H), 6.98 (d, *J* = 8 Hz, 1H), 6.91 (t, *J* = 8.2 Hz, 6H), 1.97 (s, 6 H), 1.9 (d, *J* = 16.7 Hz, 3H).

#### PI C.



Anal. calcd for C<sub>68</sub>H<sub>39</sub>F<sub>6</sub>N<sub>2</sub>O<sub>9</sub>P (1173.01 g/mol): C, 69.63%; H, 3.35%; F, 9.72%; N, 2.39%; O, 12.28%; P, 2.64%. %; found: C, 69.66%; H, 3.33%; F, 9.70%; N, 2.36%; O, 12.30%, P, 2.60%. FTIR (KBr, cm<sup>-1</sup>): 3366 (N–H stretching), 1684 (>C=O stretching), 1236 (O=P), 920 (P–O–Ph stretching). <sup>1</sup>H NMR (CDCl<sub>3</sub>, 600 MHz, δ ppm): 7.92 (m, 2H), 7.86 (t, *J* = 8.3 Hz, 4H), 7.75 (d, *J* = 8 Hz, 2H), 7.71 (d, *J* = 8 Hz, 4H), 7.64 (t, *J* = 7.8 Hz, 1H), 7.57 (d, *J* = 8 Hz, 4H), 7.52 (t, *J* = 7.7 Hz, 1H), 7.48 (s, 1H), 7.38 (d, *J* = 8.2 Hz, 6H), 7.31 (d, *J* = 8.2 Hz, 5H), 7.3 (s, 1H), 7.16 (d, *J* = 7.8 Hz, 1H), 7.10 (d, *J* = 8.0 Hz, 1H), 7.03 (d, *J* = 7.8 Hz, 1H), 6.97 (d, *J* = 8 Hz, 1H), 6.9 (t, *J* = 7.8 Hz, 1H), 1.79 (d, *J* = 16.8 Hz, 3H).

#### PI D.



Anal. calcd for C<sub>69</sub>H<sub>39</sub>F<sub>6</sub>N<sub>2</sub>O<sub>9</sub>P (1185.02 g/mol): C, 69.63%; H, 3.32%; F, 9.62%; N, 2.36%; O, 12.15%; P, 2.61%. %; found: C, 69.61%; H, 3.35%; F, 9.59%; N, 2.33%; O, 12.27%, P, 2.63%. FTIR (KBr, cm<sup>-1</sup>): 3360 (N–H stretching), 1688 (>C=O stretching), 1236 (O=P), 919 (P–O–Ph stretching).

**Measurements and Characterizations.** <sup>1</sup>H NMR spectra of the polymers were recorded in a 600 MHz NMR instrument (Bruker, Switzerland) [reference 0 ppm with tetramethylsilane (<sup>1</sup>H NMR)], and CDCl<sub>3</sub> was used as solvent. FTIR spectra of the polymers (membranes) were recorded with NEXUS Nicolet Impact-410 spectrophotometer at room temperature. Gel permeation chromatography (GPC) was performed with a Waters GPC instrument (Waters 2414). THF was used as an eluent (flow rate, 0.5 mL/min), polystyrene was used as a standard, and an RI detector was used to record the signal. Viscosity measurements ( $\eta_{inh}$ ) were performed with a Ubbelohde suspended level viscometer at 30 °C using DMF as a solvent, and the concentration of the solution was 0.5 g/dL. The wide-angle X-ray diffraction (WAXD) patterns of the polymer membranes were performed in reflection mode over the  $2\theta$  range of 5–40° at room temperature using a Ultima III X-ray diffractometer (Rigaku, Japan) at an operating voltage and current of 40 kV and 40 mA, respectively, with Cu K $\alpha$  (0.154 nm) radiation source. Differential scanning calorimetry (DSC) measurements were performed on a TA Instruments DSC Q20, with 7 ± 1 mg samples at a heating or cooling rate of 20 °C/min under N<sub>2</sub> atmosphere. Glass-transition temperature ( $T_g$ ) was taken as the midpoint of the step transition of the second heating run. The thermal decomposition of polymers was investigated by thermogravimetric analysis using TGA Q50 from TA Instruments. The heating rate of the thermo-balance was 10 °C/min, and the study was performed under synthetic air (80% N<sub>2</sub> and 20% O<sub>2</sub>). The decomposition temperature  $T_{d10}$  values were taken as 10% weight loss temperature of the polymers. The stress–strain properties, such as modulus, tensile strength, and elongation at break, of the PI membranes were tested by using TINIUS OLSEN HSKS universal testing machine at a cross-head speed of 5 mm/min. Polymer films of average thickness 70

$\mu\text{m}$ , width 10 mm, and effective length 25 mm (distance between the clamps) were used for the measurements. For each polymer, the stress-strain measurements were performed with three uniform specimens and the average values are reported. The standard deviation of the measurements was below 4% of the mean value. Water absorption studies of the vacuum-dried membranes were checked by dipping the membranes in distilled water for 72 h at 30 °C. Sartorius micro balance of sensitivity  $10^{-6}$  g was used to measure the weight gains, and water absorption values were calculated using the formula: % water absorbed = [(weight of the wet film – weight of the dry film)/weight of the dry film]  $\times$  100. The dielectric constants ( $\epsilon$ ) were determined by measuring the capacitance of the PI membranes (parallel-plate capacitor method) using a YHP 4278 capacitance meter at 1 MHz at 30 °C at a relative humidity of 45. The density of the films was measured using a Wallace High Precision Densimeter-X22B (U.K.) (2,2,4-trimethylpentane displacement) at 30 °C by Archimedes' principle according to eq 2.

$$\rho = W_0 \times \rho_1 / (W_0 - W_1) \quad (2)$$

where  $\rho$ ,  $\rho_1$ ,  $W_0$ , and  $W_1$  are the density of the polymer film, density of 2,2,4-trimethylpentane ( $\sim 0.692$  g/cc), weight of polymer film in air, and weight of polymer film in 2,2,4-trimethylpentane, respectively.

The fractional free volumes (FFVs) of the polymers were calculated using eq 3.

$$\text{FFV} = (V - 1.3V_w) / V \quad (3)$$

where  $V$  is the specific volume ( $V = 1/\rho$ ), which is determined from the measured density ( $\rho$ ) values of the polymer films, and  $V_w$  is the specific van der Waals volume, which is obtained using the computer program HyperChem, version 8.0.<sup>66</sup> HyperChem computer program has developed based on the work of Bodor et al.<sup>67</sup> and Gavezzotti.<sup>68</sup> The same program has been successfully used by many researchers<sup>69</sup> where the calculation of  $V_w$  values is not possible by standard group contribution methods.

**Molecular Dynamics (MD) Simulations.** Atomistic molecular dynamics (MD) simulations were performed using the LAMMPS molecular simulation package.<sup>29,55</sup> The detailed procedure is discussed in the Supporting Information.

**Gas Permeation.** The gas-transport properties of  $\text{CO}_2$ ,  $\text{O}_2$ ,  $\text{N}_2$ , and  $\text{CH}_4$  through PI membranes (average thickness, 70  $\mu\text{m}$ ) were measured by using a permeation test system, PTS 50F-16 M, manufactured by Indian High Vacuum Pumps, India, at an applied gas pressure of 3.5 bar and 35 °C. The membranes were degassed for 24 h after placing them in a permeation cell using a turbomolecular pump, and XL grade gases from Linde India were used for permeation studies. The permeability coefficients were calculated from eq 4 and expressed in barrer.

$$P = [VdT_0/Ap_0T](dp/dt)_s \quad (4)$$

where  $P$ ,  $V$ ,  $d$ , and  $A$  are expressed as pure gas permeability in barrer (1 barrer =  $10^{-10}$  cm<sup>3</sup> (STP) cm/cm<sup>2</sup> s cmHg), downstream volume (119 cm<sup>3</sup>), thickness of the membranes (0.007 cm), and actual membrane area (12.25 cm<sup>2</sup>), respectively;  $T_0$  and  $p_0$  are the standard temperature ( $T_0 = 273.15$  K) and pressure ( $p_0 = 1.013$  bar), respectively;  $T$  and  $p_i$  are the upstream gas pressure (cmHg) and the measurement temperature (K), respectively; and  $(dp/dt)_s$  is the rate of pressure rise in the downstream chamber in the steady state. For each measurement, replicas of four specimens were used and the error of the measurements was  $\pm 5\%$  (within 1–3% for  $\text{CO}_2$  and

$\text{O}_2$  and 2–5% for  $\text{N}_2$  and  $\text{CH}_4$ ), and the gas permeability values are reported as the average of these four independent experiments. The representative plots for the 6FDA-based polyimide (PA I) are provided in the Supporting Information (Figures S1–S5). The diffusion coefficient ( $D$ ) was calculated from the time-lag " $\theta$ " value using eq 5.

$$D = d^2/6\theta \quad (5)$$

The solubility coefficient ( $S$ ) was obtained indirectly using eq 6.

$$S = P/D \quad (6)$$

The ideal permselectivity ( $\alpha_{A/B}$ ) was calculated from the ratio of the individual single gas permeabilities using eq 7.

$$\alpha_{A/B} = P_A/P_B = S_A D_A / S_B D_B \quad (7)$$

## ■ ASSOCIATED CONTENT

### Supporting Information

The Supporting Information is available free of charge on the ACS Publications website at DOI: 10.1021/acsomega.8b01364.

Molecular dynamics (MD) simulations, gas permeability measurements, output pressure versus time plots of PI A for different gases (Figures S1–S5), and references (PDF)

## ■ AUTHOR INFORMATION

### Corresponding Author

\*E-mail: susanta@matsc.iitkgp.ac.in.

### ORCID

Anaparthi Ganesh Kumar: 0000-0002-8828-7901

Susanta Banerjee: 0000-0002-0358-3198

### Notes

The authors declare no competing financial interest.

## ■ ACKNOWLEDGMENTS

R.C. acknowledges IIT Kharagpur for providing her a senior research fellowship. The financial support from the Department of Science and Technology (DST), India (Grant No. INT/RUS/RFB/P-303), is gratefully acknowledged.

## ■ REFERENCES

- (1) Carta, M.; Croad, M.; Malpass-Evans, R.; Jansen, J. C.; Bernardo, P.; Clarizia, G.; Friess, K.; Lanč, M.; McKeown, N. B. Triptycene induced enhancement of membrane gas selectivity for microporous Tröger's base polymers. *Adv. Mater.* **2014**, *26*, 3526–3531.
- (2) Koros, W. J.; Mahajan, R. Pushing the limits on possibilities for large scale gas separation: which strategies? *J. Membr. Sci.* **2000**, *175*, 181–196.
- (3) Stern, S. A. Polymers for gas separations: the next decade. *J. Membr. Sci.* **1994**, *94*, 1–65.
- (4) Maier, G. Gas separation with polymer membranes. *Angew. Chem. Int. Ed.* **1998**, *37*, 2960–2974.
- (5) Schrier, J. Carbon dioxide separation with a two-dimensional polymer membrane. *ACS Appl. Mater. Interfaces* **2012**, *4*, 3745–3752.
- (6) Sanders, D. F.; Smith, Z. P.; Guo, R.; Robeson, L. M.; McGrath, J. E.; Paul, D. R.; Freeman, B. D. Energy-efficient polymeric gas separation membranes for a sustainable future: a review. *Polymer* **2013**, *54*, 4729–4761.
- (7) Yampolskii, Y. Polymeric gas separation membranes. *Macromolecules* **2012**, *45*, 3298–3311.
- (8) Luo, S.; Stevens, K. A.; Park, J. S.; Moon, J. D.; Liu, Q.; Freeman, B. D.; Guo, R. Highly  $\text{CO}_2$ -selective gas separation membranes based on segmented copolymers of poly(ethylene oxide) reinforced with

pentiptycene-containing polyimide hard segments. *ACS Appl. Mater. Interfaces* **2016**, *8*, 2306–2317.

(9) Du, N.; Park, H. B.; Dal-Cin, M. M.; Guiver, M. D. Advances in high permeability polymeric membrane materials for CO<sub>2</sub> separations. *Energy Environ. Sci.* **2012**, *5*, 7306–7322.

(10) Freeman, B. D. Basis of permeability/selectivity tradeoff relations in polymeric gas separation membranes. *Macromolecules* **1999**, *32*, 375–380.

(11) Robeson, L. M. Correlation of separation factor versus permeability for polymeric membranes. *J. Membr. Sci.* **1991**, *62*, 165–185.

(12) Robeson, L. M. The upper bound revisited. *J. Membr. Sci.* **2008**, *320*, 390–400.

(13) Galizia, M.; Chi, W. S.; Smith, Z. P.; Merkel, T. C.; Baker, R. W.; Freeman, B. D. 50th anniversary perspective: Polymers and mixed matrix membranes for gas and vapor separation: A review and prospective opportunities. *Macromolecules* **2017**, *50*, 7809–7843.

(14) Ghanem, B. S.; McKeown, N. B.; Budd, P. M.; Selbie, J. D.; Fritsch, D. High-performance membranes from polyimides with intrinsic microporosity. *Adv. Mater.* **2008**, *20*, 2766–2771.

(15) Rahman, M. M.; Filiz, V.; Shishatskiy, S.; Abetz, C.; Georgopoulos, P.; Khan, M. M.; Neumann, S.; Abetz, V. Influence of poly(ethylene glycol) segment length on CO<sub>2</sub> permeation and stability of polyactive membranes and their nanocomposites with PEG POSS. *ACS Appl. Mater. Interfaces* **2015**, *7*, 12289–12298.

(16) Maier, G. Gas separation by polymer membranes: beyond the border. *Angew. Chem., Int. Ed.* **2013**, *52*, 4982–4984.

(17) McHattie, J. S.; Koros, W. J.; Paul, D. R. Gas transport properties of polysulphones: 1. Role of symmetry of methyl group placement on bisphenol rings. *Polymer* **1991**, *32*, 840–850.

(18) Pixton, M. R.; Paul, D. R. Gas transport properties of polyarylates part I: connector and pendant group effects. *J. Polym. Sci., Part B: Polym. Phys.* **1995**, *33*, 1135–1149.

(19) Banerjee, S. *Handbook of Specialty Fluorinated Polymers: Preparation, Properties, and Applications*; Elsevier: Oxford, U.K., 2015.

(20) Chung, I. S.; Kim, S. Y. Soluble polyimides from unsymmetrical diamine with trifluoromethyl pendent group. *Macromolecules* **2000**, *33*, 3190–3193.

(21) Qiu, Z.; Wang, J.; Zhang, Q.; Zhang, S.; Ding, M.; Gao, L. Synthesis and properties of soluble polyimides based on isomeric ditrifluoromethyl substituted 1,4-bis(4-aminophenoxy)benzene. *Polymer* **2006**, *47*, 8444–8452.

(22) Zhang, Y.; Ionov, L. Actuating Porous Polyimide Films. *ACS Appl. Mater. Interfaces* **2014**, *6*, 10072–10077.

(23) Dhara, M. G.; Banerjee, S. Fluorinated high-performance polymers: poly(arylene ether)s and aromatic polyimides containing trifluoromethyl groups. *Prog. Polym. Sci.* **2010**, *35*, 1022–1077.

(24) Maiti, S.; Banerjee, S.; Palit, S. K. Phosphorus-containing polymers. *Prog. Polym. Sci.* **1993**, *18*, 227–261.

(25) Carja, I. D.; Serbezeanu, D.; Vlad-Bubulac, T.; Hamciuc, C.; Coroaba, A.; Lisa, G.; López, C. G.; Soriano, M. F.; Pérez, V. F.; Sánchez, M. D. A straight forward, eco-friendly and cost-effective approach towards flame retardant epoxy resins. *J. Mater. Chem. A* **2014**, *2*, 16230–16241.

(26) Lin, C. H.; Chang, S. L.; Peng, L. A.; Peng, S. P.; Chuang, Y. H. Organo-soluble phosphinated polyimides from asymmetric diamines. *Polymer* **2010**, *51*, 3899–38906.

(27) Lin, C. H.; Chang, S. L.; Cheng, P. W. Dietheramine from an alkaline-stable phosphinated bisphenol for soluble polyetherimides. *Polymer* **2011**, *52*, 1249–1255.

(28) Tanaka, K.; Kita, H.; Okano, M.; Okamoto, K. I. Permeability and permselectivity of gases in fluorinated and non-fluorinated polyimides. *Polymer* **1992**, *33*, 585–592.

(29) Bisoi, S.; Mandal, A. K.; Singh, A.; Padmanabhan, V.; Banerjee, S. Soluble, optically transparent polyamides with a phosphaphenanthrene skeleton: Synthesis, characterization, gas permeation and molecular dynamics simulations. *Polym. Chem.* **2017**, *8*, 4220–4232.

(30) Koley, T.; Bandyopadhyay, P.; Mohanty, A. K.; Banerjee, S. Synthesis and characterization of new aromatic poly(ether imide)s and their gas transport properties. *Eur. Polym. J.* **2013**, *49*, 4212–4223.

(31) Ghosh, A.; Sen, S. K.; Banerjee, S.; Voit, B. Solubility improvements in aromatic polyimides by macromolecular engineering. *RSC Adv.* **2012**, *2*, S900–S926.

(32) Sen, S. K.; Banerjee, S. High T<sub>g</sub> processable fluorinated polyimides containing benzoisindoleone unit and evaluation of their gas transport properties. *RSC Adv.* **2012**, *2*, 6274–6289.

(33) Ghosh, S.; Banerjee, S. 9-Alkylated fluorene-based poly(ether imide)s and their gas transport properties. *J. Membr. Sci.* **2016**, *497*, 172–182.

(34) Banerjee, S.; Bera, D. Polycondensation Materials Containing Bulky Side Groups. In *Membranes for Gas and Vapor Separation*; Yampolskii, Y., Finkelshtein, E., Eds.; John Wiley & Sons Ltd.: Hoboken, 2017; pp 223–269.

(35) Shantarovich, V. P.; Kevdina, I. B.; Yampolskii, Y. P.; Alentiev, A. Y. Positron annihilation lifetime study of high and low free volume glassy polymers: Effects of free volume sizes on the permeability and permselectivity. *Macromolecules* **2000**, *33*, 7453–7466.

(36) Takekoshi, T., Ed. *Kirk-Othmer Encyclopedia of Chemical Technology*; Wiley: New York, 1996; Vol. 19, p 813.

(37) Tao, L.; Yang, H.; Liu, J.; Fan, L.; Yang, S. Synthesis and characterization of highly optical transparent and low dielectric constant fluorinated polyimides. *Polymer* **2009**, *50*, 6009–6018.

(38) Kute, V.; Banerjee, S. Polyimides 7: Synthesis, characterization, and properties of novel soluble semifluorinated poly(ether imide)s. *J. Appl. Polym. Sci.* **2007**, *103*, 3025–3044.

(39) Wang, Z.; Chen, T.; Xu, J. Hydrogen-bonding in cardo copoly(aryl ether ketone)s and its effects on the gas permeation behavior. *Macromolecules* **2007**, *40*, 3238–3245.

(40) Isfahani, A. P.; Sadeghi, M.; Wakimoto, K.; Shrestha, B. B.; Bagheri, R.; Sivaniah, E.; Ghalei, B. Pentiptycene-based polyurethane with enhanced mechanical properties and CO<sub>2</sub>-plasticization resistance for thin film gas separation membranes. *ACS Appl. Mater. Interfaces* **2018**, *10*, 17366–17374.

(41) Bera, D.; Bandyopadhyay, P.; Ghosh, S.; Banerjee, S. Gas transport properties of aromatic polyamides containing adamantyl moiety. *J. Membr. Sci.* **2014**, *453*, 175–191.

(42) Bandyopadhyay, P.; Banerjee, S. Spiro [fluorene-9,9'-xanthene] containing fluorinated poly(ether amide)s: Synthesis, characterization and gas transport properties. *Eur. Polym. J.* **2015**, *69*, 140–155.

(43) Wang, Z.; Wang, D.; Jin, J. Microporous polyimides with rationally designed chain structure achieving high performance for gas separation. *Macromolecules* **2014**, *47*, 7477–7483.

(44) Ghosh, S.; Bera, D.; Bandyopadhyay, P.; Banerjee, S. Effect of introduction of cardo cyclohexylidene moiety on gas transport properties of fluorinated poly(arylene ether)s. *Eur. Polym. J.* **2014**, *52*, 207–217.

(45) Kammakakam, I.; Kim, H. W.; Nam, S.; Park, H. B.; Kim, T. H. Alkyl imidazolium-functionalized cardo-based poly(ether ketone)s as novel polymer membranes for O<sub>2</sub>/N<sub>2</sub> and CO<sub>2</sub>/N<sub>2</sub> separations. *Polymer* **2013**, *54*, 3534–3541.

(46) Koros, W. J.; Fleming, G. K. Membrane-based gas separation. *J. Membr. Sci.* **1993**, *83*, 1–80.

(47) Dasgupta, B.; Sen, S. K.; Banerjee, S. Gas transport properties of fluorinated poly(ether imide) membranes containing indan moiety in the main chain. *J. Membr. Sci.* **2009**, *345*, 249–256.

(48) Bisoi, S.; Mandal, A. K.; Padmanabhan, V.; Banerjee, S. Aromatic polyamides containing trityl substituted triphenylamine: Gas transport properties and molecular dynamics simulations. *J. Membr. Sci.* **2017**, *522*, 77–90.

(49) Swaidan, R.; Ghanem, B.; Pinnau, I. Fine-tuned intrinsically ultramicroporous polymers redefine the permeability/selectivity upper bounds of membrane-based air and hydrogen separations. *ACS Macro Lett.* **2015**, *4*, 947–951.

(50) Robeson, L. M.; Dose, M. E.; Freeman, B. D.; Paul, D. R. Analysis of the transport properties of thermally rearranged (TR) polymers and

polymers of intrinsic microporosity (PIM) relative to upper bound performance. *J. Membr. Sci.* **2017**, *525*, 18–24.

(51) Guiver, M. D.; Robertson, G. P.; Dai, Y.; Bilodeau, F.; Kang, Y. S.; Lee, K. J.; Jho, J. Y.; Won, J. Structural characterization and gas-transport properties of brominated matrimid polyimide. *J. Polym. Sci., Part A: Polym. Chem.* **2002**, *40*, 4193–4204.

(52) Barbari, T. A.; Koros, W. J.; Paul, D. R. Polymeric membranes based on bisphenol-A for gas separations. *J. Membr. Sci.* **1989**, *42*, 69–86.

(53) Xia, J.; Liu, S.; Pallathadka, P. K.; Chng, M. L.; Chung, T. S. Structural determination of Extrem XH 1015 and its gas permeability comparison with polysulfone and ultem via molecular simulation. *Ind. Eng. Chem. Res.* **2010**, *49*, 12014–12021.

(54) Wiegand, J. R.; Smith, Z. P.; Liu, Q.; Patterson, C. T.; Freeman, B. D.; Guo, R. Synthesis and characterization of triptycene-based polyimides with tunable high fractional free volume for gas separation membranes. *J. Mater. Chem. A* **2014**, *2*, 13309–13320.

(55) Bera, D.; Padmanabhan, V.; Banerjee, S. Highly gas permeable polyamides based on substituted triphenylamine. *Macromolecules* **2015**, *48*, 4541–4554.

(56) Stern, S. A.; Liu, Y.; Feld, W. A. Structure/permeability relationships of polyimides with branched or extended diamine moieties. *J. Polym. Sci., Part B: Polym. Phys.* **1993**, *31*, 939–951.

(57) Cecopieri-Gómez, M. L.; Palacios-Alquisira, J.; Dominguez, J. M. On the limits of gas separation in CO<sub>2</sub>/CH<sub>4</sub>, N<sub>2</sub>/CH<sub>4</sub> and CO<sub>2</sub>/N<sub>2</sub> binary mixtures using polyimide membranes. *J. Membr. Sci.* **2007**, *293*, 53–65.

(58) Kazarian, S. G.; Vincent, M. F.; Bright, F. V.; Liotta, C. L.; Eckert, C. A. Specific intermolecular interaction of carbon dioxide with polymers. *J. Am. Chem. Soc.* **1996**, *118*, 1729–1736.

(59) Hofmann, D.; Entrialgo-Castano, M.; Lerbret, A.; Heuchel, M.; Yampolskii, Y. Molecular modeling investigation of free volume distributions in stiff chain polymers with conventional and ultrahigh free volume: comparison between molecular modeling and positron lifetime studies. *Macromolecules* **2003**, *36*, 8528–8538.

(60) Heuchel, M.; Hofmann, D.; Pullumbi, P. Molecular modeling of small-molecule permeation in polyimides and its correlation to free-volume distributions. *Macromolecules* **2004**, *37*, 201–214.

(61) Maya, E. M.; Yoldi, I. G.; Lozano, A. E.; de la Campa, J. G.; de Abajo, J. Synthesis, characterization, and gas separation properties of novel copolyimides containing adamantyl ester pendant groups. *Macromolecules* **2011**, *44*, 2780–2790.

(62) Nagel, C.; Günther-Schade, K.; Fritsch, D.; Strunskus, T.; Faupel, F. Free volume and transport properties in highly selective polymer membranes. *Macromolecules* **2002**, *35*, 2071–2077.

(63) Chang, K. S.; Wu, Z. C.; Kim, S.; Tung, K. L.; Lee, Y. M.; Lin, Y. F.; Lai, J. Y. Molecular modeling of poly(benzoxazole-co-imide) membranes: A structure characterization and performance investigation. *J. Membr. Sci.* **2014**, *454*, 1–11.

(64) Tocci, E.; De Lorenzo, L.; Bernardo, P.; Clarizia, G.; Bazzarelli, F.; Mckeown, N. B.; Carta, M.; Malpass-Evans, R.; Friess, K.; Pilnáček, K.; Lanč, M.; et al. Molecular Modeling and Gas Permeation Properties of a Polymer of Intrinsic Microporosity Composed of Ethanoanthracene and Tröger's Base Units. *Macromolecules* **2014**, *47*, 7900–7916.

(65) Neyertz, S.; Brown, D. Influence of system size in molecular dynamics simulations of gas permeation in glassy polymers. *Macromolecules* **2004**, *37*, 10109–10122.

(66) *HyperChem(TM) Professional*, version 7.5; Hypercube, Inc.: Gainesville.

(67) Bodor, N.; Gabanyi, Z.; Wong, C. K. A new method for the estimation of partition coefficient. *J. Am. Chem. Soc.* **1989**, *111*, 3783–3786.

(68) Gavezzotti, A. The calculation of molecular volumes and the use of volume analysis in the investigation of structured media and of solid-state organic reactivity. *J. Am. Chem. Soc.* **1983**, *105*, 5220–5225.

(69) Espeso, J.; Lozano, A. E.; José, G.; de Abajo, J. Effect of substituents on the permeation properties of polyamide membranes. *J. Membr. Sci.* **2006**, *280*, 659–665.